Harnessing the central dogma for stringent multi-level control of gene expression

F. Veronica Greco[1], Claire S. Grierson[1,2] and Thomas E. Gorochowski[1,2,*]

[1] School of Biological Sciences, University of Bristol, Tyndall Avenue, Bristol BS8 1TQ, UK

[2] BrisSynBio, University of Bristol, Tyndall Avenue, Bristol BS8 1TQ, UK

* Correspondence should be addressed to T.E.G. (thomas.gorochowski@bristol.ac.uk)

Keywords: gene expression; transcription; translation; genetic circuit; synthetic biology; regulatory motif; feed forward loop; control.

Abstract

Strictly controlled inducible gene expression is crucial when engineering biological systems where even tiny amounts of a protein have a large impact on function or host cell viability. In these cases, leaky protein production must be avoided at all costs. Here, we demonstrate how the central dogma offers a simple way to effectively address this challenge. By simultaneously regulating both transcriptional and translational levels, we show how basal expression of an inducible system can be reduced to virtually undetectable levels, with minimal impact on the maximum induced expression rate achieved. Using this approach, we create several stringent expression systems displaying >1000-fold change in their output after induction. Furthermore, we find that multi-level regulation is able to supress transcriptional noise and create a digital-like switch when transitioning between ‘on’ and ‘off’ states. This work provides foundational knowledge and a genetic toolkit of parts to create multi-level gene expression controllers for those working with toxic genes or requiring precise regulation and propagation of cellular signals. It also demonstrates the value of exploring more complex and diverse regulatory designs for synthetic biology.

Introduction

Since the development of the first inducible systems in the early 1980s (de Boer et al., 1983), the ability to dynamically control gene expression through the use of small molecules (Gallivan, 2007), light (Baumschlager et al., 2017; Castillo-Hair et al., 2019), and other signals (Sen et al., 2017) has revolutionized biotechnology. From controlling shifts between cell growth and protein production stages during large-scale fermentations (Sivashanmugam et al., 2009), to the detailed characterization of genetic parts and circuitry (Olson et al., 2014), the control of gene expression underpins a huge variety of applications. However, while switching expression of a gene 'on' or 'off' is conceptually simple, it is rare for genes to have such discrete states or ever be completely silenced. Stochastic effects (Elowitz et al., 2002; Raj and van Oudenaarden, 2008) and leaky expression are widespread and potentially important for adaptation in natural systems but can wreak havoc in engineered systems where genes are toxic to a host or responses are highly sensitive and easily triggered by mistake (Rosano and Ceccarelli, 2014; Süel et al., 2006).

Early systems for controlling gene expression relied on the repurposing of native regulatory components such as transcription factors. One of the most widely used is the P_{tac} system (de Boer et al., 1983). This consists of a constitutively expressed LacI repressor that can form dimers and tetramers to strongly bind operator sites within a P_{tac} promoter sequence and sterically block initiation of RNA polymerase (RNAP). LacI is sensitive to Isopropyl β-d-1-thiogalactopyranoside (IPTG) and at high concentrations, the DNA binding activity of LacI is abolished. This lifts repression of P_{tac} and leads to strong transcription of genes regulated by this promoter. While in most cases such systems offer strong repression, because such regulatory systems focus on a single step during protein synthesis (i.e. transcription), they are vulnerable to fluctuations in regulator production and the stochastic nature of biochemical reactions during gene expression (Raj and van Oudenaarden, 2008).

Over the past decade, synthetic biologists have developed more advanced methods to control gene expression. These include engineered regulators based on DNA binding proteins such as zinc fingers (Khalil et al., 2012), TALENs (Deng et al., 2014) and CRISPRi (Gilbert et al., 2014), RNA-RNA interactions (Bartoli et al., 2020; Chappell et al., 2017; Green et al., 2014), post-transcriptional/translational processes such as RNA and protein degradation (Cameron and Collins, 2014), as well as using directed evolution to optimize existing inducible systems (Meyer et al., 2019). This offers a wealth of options to more strictly regulate gene expression through the coupling of multiple forms of regulation (e.g. affecting both transcription and translation of a gene) to reduce unwanted expression and improve the robustness of a system to component failure. However, few examples of such multi-level regulation have been implemented to date (Westbrook and Lucks, 2017). This has resulted in

an unclear picture of how best stringent multi-level control can be achieved and the trade-offs that exist between performance, regulatory complexity, and cellular burden when designing these systems.

Here, we address this problem by systematically studying the combined use of transcriptional and translational regulators to stringently control protein expression. Using a combination of mathematical modelling and a combinatorial genetic assembly method, we are able to design, build and test a variety of synthetic multi-level controllers (MLCs) and elucidate the relative performance of each. These controllers all implement a coherent type 1 feed-forward loop (C1-FFL) regulatory motif (**Figure 1A**) that is commonly found in natural genetic systems and is known to enable more stringent control of an output but is rarely used when designing new expression systems (Mangan and Alon, 2003). We show how MLCs offer advantages for many applications spanning the stringent control of protein expression to the accurate propagation of information in a cell (Beal, 2015; Nielsen et al., 2016) and demonstrate how applying modern synthetic biology tools to even simple regulatory systems can offer paths towards the precise and reliable control of biological systems.

Results

Stringent control of gene expression by harnessing the central dogma

In most synthetic genetic circuits, control of gene expression is achieved through the use of a single type of regulation (**Figure 1A**), with control of transcription predominantly used. While this type of single-level control (SLC; **Figure 1B**) is often sufficient for many applications, the central dogma naturally lends itself to more stringent multi-level regulation where both transcription and translation are controlled simultaneously by different types of regulator (e.g. via transcription factors and RNA-based translational switches). Such multi-level control (MLC; **Figure 1C**) can be generalised by a genetic design that consists of an *L1* gene encoding a level 1 transcriptional regulator with cognate promoter P_{L1}, and an *L2* gene encoding a level 2 translational regulator. Both *L2* and the gene of interest (GOI) are separately transcribed by P_{L1} promoters and the product of *L2* activates translation of the GOI transcript. This MLC encapsulates a coherent type 1 feed forward loop (C1-FFL) in which both *L1* and *L2* are necessary for production of the GOI.

To explore the possible benefits of this regulatory motif, we developed mathematical models to capture how the rate of production of a GOI varied in response to differing concentrations of an input inducer for both the SLC and MLC designs (**Supplementary Note 1**; **Supplementary Data 1**). We generated steady state response functions by simulating the models using biologically realistic parameters (**Supplementary Table 1**) over a range of different input IPTG concentrations. As expected, the output production rate displayed a

sigmoidal shape with both controllers reaching near identical maximum rates at high input IPTG concentrations (**Figure 1D**). The main difference was that the MLC design displayed a 50-fold lower output than the direct controller at low IPTG concentrations, leading to significantly reduced basal expression when no input was present (**Figure 1D**). This caused the MLC design to have both an increased dynamic range and fold-change between 'off' and 'on' states when compared to the SLC design.

We also simulated the output protein production rate for both models when exposed to a range of dynamic inputs. These included delta functions, as well as pulse and step inputs (**Figure 1E**). Simulations showed that both types of controller displayed virtually identical output responses for both the pulse and step inputs, with only a small reduction in output expression rate for the MLC that matched its lower basal expression level. However, significant differences were observed in the responses to the delta function input. While the SLC led to moderate sized pulses in output, the MLC design fully suppressed all output activity with only tiny fluctuations in the output expression rate observed. The behaviour of the MLC arose from the need for both *L1* and *L2* to be expressed to sufficiently high levels for expression of the GOI to be triggered. The short pulses of expression caused by the delta function input were insufficient to cause this switch and allowed the MLC to effectively filter out these transient events in its input.

The ability to filter out rapid fluctuations is particularly important for stringent control in systems where input promoters exhibit high levels of intrinsic noise. In such scenarios, protein levels can vary significantly across a population of cells (Elowitz et al., 2002) due to the often bursty nature of gene transcription. This is commonly seen for weak promoters where intrinsic noise dominates. Rather than the activity of a weak promoter being uniformly low, it instead displays short bursts of strong activity separated by long periods of inactivity (Elowitz et al., 2002; Golding et al., 2005). Across a population this averages out to a low overall expression level, but large variability is present between cells. As seen for the delta function inputs, such input profiles driving the SLC will lead to large fluctuations in the output. However, because intrinsic promoter noise is specific to an individual promoter and uncorrelated between multiple identical versions of a promoter within a construct, the MLC design which contains two copies of the input promoter P_{L1} should find that a burst of expression from one P_{L1} promoter is highly unlikely to occur at the same time as a burst from the other. Therefore, the MLC will suppress noise in the output.

To test this hypothesis, we generated accurate time-series promoter activity profiles based on a two-state model (Golding et al., 2005) where the mean length of time a promoter was in an 'on' active and 'off' silent state (Δt_{ON} and Δt_{OFF}, respectively) were $\langle \Delta t_{ON} \rangle$ = 6 min and $\langle \Delta t_{OFF} \rangle$ = 37 min. These values were taken from previous experimental measurements in *E. coli* (Golding et al., 2005). We also set the activity of the P_{L1} promoter when in an 'on' state to

a biologically realistic 0.25 RNAP/min. Independent time-series were generated for each P_{L1} promoter in the MLC and only one of these was used for the SLC where only a single P_{L1} promoter is present. These profiles were then fed into our existing dynamic models and the responses of the systems simulated. We found that the output production rate for the SLC saw large increases, especially where the input consisted of longer bursts of activity or several bursts in short succession (**Figure 1F**). In comparison, the MLC fully supressed all output production making it an excellent filter of intrinsic promoter noise.

A genetic template to explore multi-level gene regulation

There are many ways that an MLC could be implemented biologically. Furthermore, when implementing such a controller it is often necessary to switch the input that is used and internal regulators such that multiple controllers can be used simultaneously within the same cell. To meet these requirements, we developed an 8-part genetic template and toolkit of parts to allow for the rapid combinatorial assembly of MLCs (**Figure 2A**). The design enables both single and multi-level regulation, has the option to introduce protein tags for further post-translational control of the GOI (e.g. through signalled degradation) and is structured to minimise the chance for transcriptional readthrough to cause unwanted expression of the component parts. The toolkit comprises of 8 types of part plasmid (pA–pH) and a backbone plasmid (pMLC-BB1) in which the final MLC design is inserted (**Supplementary Data 2**). Assembly is performed using a standard one-pot Golden Gate reaction with individual blocks designed to use 4 bp overhangs with minimal cross reactivity to ensure the correct and efficient ligation of parts (Woodruff et al., 2016). Furthermore, rapid screening of successful inserts is enabled by the drop-out of an orange fluorescent protein (*ofp*) expression unit (Engler et al., 2009) (**Supplementary Note 2**).

Using this toolkit, we aimed to compare the *in vivo* behaviours of different SLC and MLC designs with a focus on the different mechanisms that could be used for *L2* control and the affect these might have on overall performance. For the SLC design we chose the widely used P_{tac} system introduced earlier (**Figure 2C**). To simplify comparisons, we also used the P_{tac} system for *L1* control in all the MLC designs and combined it with three different RNA-based *L2* regulators. These included a toehold switch (THS; **Figure 2D**) (Green et al., 2014, 2017), a small transcription activating RNA (STAR; **Figure 2E**) (Chappell et al., 2015), and a dual control system (DC; **Figure 2F**) (Westbrook and Lucks, 2017).

The THS regulator encodes a structural component followed by a ribosome binding site (RBS) that is used to drive translation of the GOI (**Figure 2D**). The structural region is designed to form a strong hairpin loop that when transcribed hinders the ability for ribosomes to bind the RBS, and thus inhibits translation. Translation is activated by expression of a complementary small RNA (sRNA) trigger that hybridizes to a short unstructured region of the

THS which causes a breakdown in its secondary structure. This conformational change allows ribosomes to bind the RBS and translation of the GOI to proceed. THSs were selected because they offer strong repression of translation, can be designed computationally, and large libraries of designs exist with minimal crosstalk when used together (Green et al., 2014, 2017).

Unlike the THS, the STAR regulator works at a transcriptional level. The STAR's target is placed before an RBS in the 5' untranslated region (UTR) of the GOI (**Figure 2E**). This forms an intrinsic terminator when transcribed and inhibits GOI expression. Activation is achieved by expression of the STAR RNA, which interacts with the target, prevents terminator formation and thus allows for expression of the downstream GOI. Similar to THSs, STARs have been shown to offer strong repression and there exist large libraries of orthogonal variants (Chappell et al., 2015, 2017).

Finally, the DC regulator combines both transcriptional and translational control by modifying the pT181 attenuator (Westbrook and Lucks, 2017). The DC target is placed in the 5'-UTR of the GOI and encodes an intrinsic terminator that includes the RBS (**Figure 2F**). When transcribed, the intrinsic terminator not only halts transcription, but also represses translation by causing the RBS to form a strong RNA secondary structure making it inaccessible to the ribosome. Activation is achieved by expression of a STAR, which interacts with the target, both preventing terminator formation and causing a conformational change in the RNA structure that makes the RBS accessible for translation initiation. The DC regulator was chosen due to this combined regulatory action which has been shown to produce strong repression (Westbrook and Lucks, 2017). However, to date, only a single of these regulators has been created, limiting future applications.

DNA encoding parts for each of these regulatory systems was synthesised and our toolkit used to assemble the SLC and three MLC designs. Superfolder green fluorescent protein (*gfp*) was chosen as the GOI to allow for the measurement of output expression in single cells using flow cytometry.

Performance comparison of the controllers

To characterise the performances of the controllers, we transformed *Escherichia coli* cells with each construct and measured GFP fluorescence using flow cytometry for 'off' and 'on' input states. As P_{tac} was used as an input for all the designs, this corresponded to growing the cells in either 0 or 1 mM IPTG, respectively (**Methods**). Data from these experiments was then used to calculate the dynamic range and fold change in output GFP fluorescence (**Table 1**).

We found a clear separation between output states for all designs with little variation between biological replicates (**Figures 3A**). All MLCs (THS, STAR and DC) reached higher expression levels than the P_{tac} SLC, and the THS and DC designs achieved large >1000-fold

changes between output states. Notably, while the STAR design reached a much higher 'on' state than the P_{tac} design, the STARs high levels of basal (leaky) expression when no input was present resulted in a 43% lower fold change (**Table 1**).

A challenge when calculating these measures (especially fold change) is the ability to accurately quantify very low level of output GFP fluorescence, which are near or identical to the autofluorescence of the cells. To better understand this aspect, we measured the GFP autofluorescence of untransformed *E. coli* cells, performing 11 biological replicates to estimate a fluorescence distribution that could be used as an approximate detection limit. Overlaying the average and standard deviation of the cell autofluorescence onto our results (**Figure 3A**, dashed line and grey shaded region), we found that the 'off' states for the P_{tac}, THS and DC designs all fell within this region and very close to the average suggesting they have virtually no leaky expression at all.

While comparisons of average expression levels between 'on' and 'off' states are useful, they are not able to capture the role of cell-to-cell variability inherent in all gene expression (Raj and van Oudenaarden, 2008). Such variation is crucial when assessing the performance of stringent expression systems because even though average output states might be sufficiently separated to be distinguished, cell-to-cell variation across a population can lead to overlaps in the output distributions. Cells falling in this overlap are impossible to classify resulting in some cells with an undetermined state. Engineers have developed measures to help characterise the strength and quality of a signal (i.e. the ability to distinguish 'on' and 'off' output states) with the Signal to Noise Ratio (SNR) commonly used in other fields such as electronics. SNR has also recently been adapted for use when studying engineered genetic systems making it easier to understand how the quality of signals in a circuit are maintained or degraded as they pass through various genetic devices (Beal, 2015).

Using the flow cytometry distributions, we calculated the SNR for each controller in decibel (dB) units (**Table 1**; **Methods**). We found that the P_{tac} SLC performed worst with a low SNR of 0.2 dB, corresponding to a signal barely larger than the noise. This was evident for the flow cytometry distributions where a sizable overlap in the 'on' and 'off' states was seen (**Figure 3B**). All MLCs performed better with the THS achieving an SNR >10 dB. This improved performance was also evident from the flow cytometry data with clear gaps of varying sizes between the 'on' and 'off' output distributions (**Figure 3B**).

Burden of controllers on the host cell

There is a growing awareness of the importance of considering the burden that engineered genetic parts and circuits place on their host cell (Boo et al., 2019). The introduction of a genetic construct that sequesters large quantities of shared cellular resources like ribosomes or heavily impact core metabolic fluxes can lead to reduced growth rates and trigger stress

responses that impact the function of engineered genetic parts (Ceroni et al., 2015, 2018; Gorochowski et al., 2014, 2016; Gyorgy et al., 2015; Weiße et al., 2015). When designing the MLCs, we purposefully selected RNA-based regulators as they impose a small metabolic burden on the cell (Kelly et al., 2018). However, to experimentally verify this was the case, we generated growth curves for all SLC and MLC designs (**Supplementary Figure 1**). Because the metabolic demands of the controllers would vary based on the concentration of inducer present (because varying levels of sRNA or STAR are produced), cells were exposed to 4 different IPTG concentrations (0, 0.1, 1, 10 mM) spanning the 'off' and 'on' states of the controllers.

From these growth curves, we estimated the doubling time during the exponential growth phase (**Methods**). We found that the SLC and all MLCs displayed similar doubling times of ~70 min (**Figure 3C**). Furthermore, we saw a slight decrease in the doubling times of all controllers as the IPTG concentration increased. This trend is counterintuitive given that an increasing IPTG concentrations will cause expression of the GOI and any *L2* regulators, increasing the burden on the cell. However, it is known that IPTG can have unexpected effects on cell physiology (Malakar and Venkatesh, 2012) and cause changes in plasmid stability (Gomes et al., 2020), which could lead to reduced overall burden due to fewer copies of the controller plasmid or more efficient utilisation of available nutrients by the cell.

We also measured the lag time after inoculation into fresh media before the cells entered exponential growth (**Methods**). We found differences between many of the controllers with a lag time of ~165 min for the P_{tac} and THS designs, a shorter lag time of 88 min for the DC design, and a significantly longer lag time of 373 min for the STAR design (**Figure 3D**). Closer inspection of the growth curves showed that the DC design had a consistently higher initial cell density (optical density at 600 nm of 0.07 compared to 0.04 for the THS design), which could account for the shorter lag phase (**Supplementary Figure 1**). For the STAR design the elongated lag phase coincided with a consistently longer additional time of ~100 min to reach saturation of the culture.

To better understand if the extended lag phase of the STAR-based MLC was a general feature to be expected when using this type of regulator, we rebuilt this construct using a different STAR ($STAR_2$) that had an identical initial 72 bp sequence, but unique 10 bp sequence at its 3'-end (**Supplementary Table 2**). As we would expect for such a similar design, testing of the $STAR_2$ construct showed similar performance to the initial STAR design with a good dynamic range and similar leaky expression in its output (**Table 1**; **Supplementary Figure 2**; **Methods**). However, unlike the original, the $STAR_2$ design displayed a lag phase (161 min) and doubling time (72 min) that closely matched the other MLCs. This suggests that long lag times observed for the original STAR design were likely

due to some highly specific and uncharacterised off-target interactions with endogenous cellular processes and not due to a general feature of the STAR's regulatory mechanism.

Digital-like transitions and suppression of weak input signals

Our previous modelling of the MLCs showed that in addition to improved performance in 'on' and 'off' states, the addition of the *L2* regulator also altered the response function, causing a sharper transition from an 'off' to 'on' state due to the lower basal expression, and an ability to supress low level noise in the input (**Figure 1D, E**).

To assess if these features were present, we generated response functions of the controllers by growing the cells in varying concentrations of input inducer and measuring steady state output GFP fluorescence. The sharpness of the transition is captured by the cooperativity of Hill function fits to this data. We found that in comparison to the P_{tac} SLC, both the THS and STAR MLCs saw more than a doubling in its value from 3.4 to more than 7, while the DC design maintained an identical value (**Table 1**). High cooperativities correspond to a very sharp step-like transition between 'on' and 'off' states that is clearly evident from the response function curves (**Figure 4A**). The high non-linearity in the response functions of the THS and STAR MLCs is potentially useful for information processing tasks. In particular, implementing digital logic within cells requires clear 'on' and 'off' states and limited chance for signals to reside at intermediate states. Sharp transitions in the response function ensure that there is less room for an input to fall at an intermediate point during the transition, ensuring an 'on' or 'off' state is always given. Furthermore, a high non-linearity can also be exploited to generate bimodality. For example, if a noisy input is positioned to span the transition point in the response function, a population of cells will have large groups of cells in 'on' and 'off' states, with much fewer in intermediate states because of the sharp transition and small probability of falling in this small region.

To quantify the ability of each MLC to supress low level input noise, we further analysed the response functions. A difficulty when comparing the response functions is the large differences observed in the dynamic range of each design. Given that the promoter driving transcription for each MLC is identical (P_{tac}), this discrepancy comes from differing *gfp* translation rates controlled by the associated ribosome binding site. These do differ in sequence and strength for each design and in some cases are specific and integral to the RNA regulator's function. Therefore, to allow for comparisons, we normalised the output of each MLC to its maximum output and used data from the P_{tac} SLC to estimate the input activity of the P_{tac} promoter used in each controller. If no secondary regulation was present (as in the SLC), then we would expect the normalised input and output to follow a straight line where one equals the other (see Ptac design in **Figure 4B**). However, if the secondary regulation

supresses the input P_{tac} activity then a lower normalised output to input will be seen, and conversely, an amplification of the input will lead to a higher normalised output to input.

Using this approach, we assessed the responses of each MLC and found that all caused a suppression of low levels of input promoter activity, while an amplification of higher input activities. This effect was most prominent for the THS and STAR designs, with both able to ensure controller output is maintained below 1% even when the input promoter reaches 3.5% activity (**Figure 4B**, insert). These results confirm the findings of our modelling and demonstrate the potential for using MLCs to filter out unwanted input activity in noisy environments.

Discussion

In this work we have shown how multi-level control of gene expression offers a means to more stringently regulate gene expression. By harnessing the multi-step process of transcription and translation that underpins the central dogma of biology and simultaneously regulating both processes in response to an input signal, we demonstrate through modelling (**Figure 1**) and experiments (**Figures 2** and **3**) how inducible expression systems can be created with virtually undetectable leaky expression when in an 'off' state, while also maintaining high expression rates once induced. Furthermore, we have shown that multi-level regulation creates a more digital-like switch when transitioning between 'off' and 'on' states and supresses low-level transcriptional noise (**Figure 4**), both of which are valuable properties when developing genetic systems for information processing or when highly toxic products or excitable systems act as downstream products.

Our top MLC design, which makes use of a THS for *L2* regulation, achieved >2000-fold change in output upon induction and displayed a 10 dB SNR (**Table 1**) making it one of the most tightly controlled and high-performance induction systems built to date. Furthermore, the flexibility of our modular genetic toolkit for assembling new multi-level controllers (**Figure 2**), and the availability of many other THSs, makes it easy to develop additional orthogonal MLCs that could be used in parallel within the same cell. It is worth noting that the underlying P_{tac} promoter that the THS MLC uses, achieved only a 93-fold change and 0.2 dB SNR when used alone as an SLC. Therefore, employing the multi-level regulatory approach outlined in this work could offer a means to greatly improve the performance of many existing low-performance transcriptional sensors, without any need to modify the transcription factors or promoter sequences making up these devices.

With the improvements we see when employing multi-level regulation, it is likely no coincidence that small interfering RNAs (siRNAs) are also widely used by bacteria to refine the regulation of many endogenous processes (Gottesman, 2005; Storz et al., 2004; Waters

and Storz, 2009). RNAs are perfectly tailored for this task, imposing a small metabolic burden and offering a fast response. In this work, we selected synthetic RNA-based regulators that function through RNA-RNA hybridisation alone. While this reduces our dependencies on other cellular machinery and makes them easier to transfer between strains/organisms, it is known that many endogenous siRNA regulators employ protein chaperones such as Hfq to increase their binding affinity to targets and strengthen their regulatory effect (Soper et al., 2010). It would be interesting to explore the use of synthetic regulators that make use of these chaperones (Kelly et al., 2018) or exploit recent advances in the RNA part design (Chappell et al., 2017) to see whether further improvements in performance are possible.

The stringent regulation of our controllers is achieved by incorporating a C1-FFL regulatory motif that is known to be evolutionarily selected in many natural and engineered systems (Milo et al., 2002) and can be used to implement many useful functionalities (Mangan and Alon, 2003). More recent work has also demonstrated the importance of interconnections and clustering of many motifs in coordinating more complex behaviours (Gorochowski et al., 2018; S. Dunn et al., 2019). While this work focused on demonstrating that transcriptional and translational regulation can fit neatly into a C1-FFL structure, an intriguing future direction would be to explore how these higher-level structures (e.g. motif clusters or higher-level network structures) might be implemented using the approaches outlined in this work to aid the coordination of multiple interrelated processes in parallel.

This study started with the goal of more stringently controlling gene expression. However, through the design of our MLCs it became evident that the more intricate regulatory designs we built had many other benefits. Synthetic biology to date has often focused on simplifying complexity and reducing systems to their minimal parts. Our findings indicate that complementary studies exploring the complexification of synthetic regulatory systems might also reap rewards allowing us to more efficiently exploit the capabilities of biology by combining many diverse processes and parts in unison. The genetic toolkit presented here offers a starting point for such studies focused on the fundamental processes of transcription and translation.

Methods

Strains, media and chemicals

All cloning and characterization of genetic constructs was performed using *Escherichia coli* strain DH10-β (Δ(ara-leu) 7697 araD139 fhuA ΔlacX74 galK16 galE15 e14- ϕ80dlacZΔM15 recA1 relA1 endA1 nupG rpsL (StrR) rph spoT1 Δ(mrr-hsdRMS-mcrBC) (New England Biolabs, C3019I). Cells were grown in DH10-β outgrowth medium (New England Biolabs, B9035S) for transformation, LB broth (Sigma-Aldrich, L3522) for general propagation, and M9

minimal media supplemented with glucose (6.78 g/L Na_2HPO_4, 3 g/L KH_2PO_4, 1 g/L NH_4Cl, 0.5 g/L NaCl (Sigma-Aldrich, M6030), 0.34 g/L thiamine hydrochloride (Sigma T4625), 0.4% D-glucose (Sigma-Aldrich, G7528), 0.2% casamino acids (Acros, AC61204-5000), 2 mM $MgSO_4$ (Acros, 213115000), and 0.1 mM $CaCl_2$ (Sigma-Aldrich, C8106)) for characterization experiments. Antibiotic selection was performed using 100 µg/mL ampicillin (Sigma-Aldrich, A9518) and 50 µg/mL kanamycin (Sigma-Aldrich, K1637). Induction of the expression systems was performed using varying concentrations of isopropyl β-D-1-thiogalactopyranoside (IPTG) (Sigma-Aldrich, I6758).

Assembly of controllers

All part plasmids were either directly synthesised (GeneArt, Thermo Fisher Scientific) or assembled as complementary single-stranded DNA oligos annealed together. Controllers consisting of 8-parts (pA–pH) plus a backbone (pMLC-BB1) were assembled using a standard Golden-Gate cloning method (**Figure 2B**) (Engler et al., 2009). Briefly, for each assembly, we started from the 18.5 ng of required part plasmids (pA–pH) and 18.5 ng of the backbone (pMLC-BB1) to be added to a 5 µL Golden-Gate reaction. The standard manufacturer's reaction conditions were used, but at a quarter of their normal volume (New England Biolabs, E1601). 2 µL of this reaction mix was then used to transform 12.5 µL of chemically competent DH10-β cells (New England Biolabs, C3019) for further experiments. All assembled constructs were sequence verified by Sanger sequencing (Eurofins Genomics). Annotated sequences of all part and backbone plasmids and assembled controllers are provided in GenBank format in **Supplementary Data 2**.

Characterisation experiments

Single colonies of cells transformed with an appropriate genetic construct were inoculated in 200 µL M9 media supplemented with glucose and kanamycin for selection in a 96-well microtiter plate (Thermo Fisher Scientific, 249952). Cultures were grown for 14 hours in a shaking incubator (Stuart, S1505) at 37 °C and 1250 rpm. Following this, the cultures were diluted 3:40 (15 µL in 185 µL) in M9 media supplemented with glucose, kanamycin for selection and IPTG for induction in a new 96-well microtiter plate and grown for a further 4 hours under the same conditions. Finally, the cultures were further diluted 1:10 (10 µL into 90 µL) in phosphate-buffered saline (PBS) (Gibco,18912-014) containing 2 mg/mL kanamycin to halt protein translation. These samples were incubated at room temperature for 1 hour to allow for full maturation of GFP before flow cytometry was performed.

Flow cytometry

Measurements of GFP fluorescence in single cells was performed using an Acea Biosciences NovoCyte 3000 flow cytometer equipped with a NovoSampler to allow for automated collection of samples from a 96-well microtiter plate. Data collection was performed using the NovoExpress software. Cells were excited using a 488 nm laser and GFP fluorescence measurements taken using a 530 nm detector. At least 10^6 events were captured per sample. In addition, to enable conversion of GFP fluorescence into calibrated MEFL units (Castillo-Hair et al., 2016) a single well per plate contained 15 µL of 8-peak Rainbow Calibration Particles (Spherotech, RCP-30-5A) diluted into 200 µL PBS. Automated gating of events and conversion of GFP fluorescence into MEFL units was performed using the forward (FSC) and side scatter (SSC) channels and the FlowCal Python package version 1.2.2 with default parameters (Castillo-Hair et al., 2016). To correct for the GFP autofluorescence of cells, *E. coli* DH10-β cells containing no genetic construct were grown in identical conditions. An average measurement of GFP fluorescence in MEFL units from three biological replicates of these cells was then subtracted from fluorescence measurements of cells containing our genetic constructs to correct for cell autofluorescence.

Plate reader measurements

Single colonies of cells transformed with an appropriate genetic construct were inoculated in 200 µL M9 media supplemented with glucose and kanamycin for selection in a 96-well microtiter plate (Thermo Fisher Scientific, 249952). Cultures were grown for 4 hours in a shaking incubator (Stuart, S1505) at 37 °C and 1250 rpm. Following this, the cultures were diluted 3:40 (15 µL in 185 µL) in M9 media supplemented with glucose, kanamycin for selection and IPTG for induction in a 96-well 190 µm clear base imaging microplate (4titude, Vision Plate™, 4ti-0223). This spectrophotometric assay was performed using a BioTek Synergy Neo2 plate reader at 37°C. Optical density at 600 nm (OD_{600}) was measured every 10 min over a 16-hour period. OD_{600} measurements were also taken from samples of M9 medium supplemented with glucose containing no cells to allow for quantification of media autofluorescence. Shaking was automated for the all the length of the experiment. Data collection was performed using the Gen5 version 3.04 software. For each time point, media autofluorescence was subtracted from the sample measurement.

Signal to noise ratio

The signal to noise ratio (SNR) in decibel (dB) units was calculated from the flow cytometry GFP fluorescence distributions using the equation (Beal, 2015)

$$\mathrm{SNR_{dB}} = 20 \cdot \log_{10} \frac{|\log_{10}(\mu_{\mathrm{ON}}/\mu_{\mathrm{OFF}})|}{2 \cdot \log_{10}(\sigma)}. \quad (8)$$

Here, μ_{ON} and μ_{OFF} are the geometric means of distributions for the ON and OFF states, respectively, and σ is the geometric standard deviation of the distribution for the OFF state. OFF and ON states correspond to cells grown in 0 and 1 mM IPTG, respectively.

Data analysis and numerical simulation

Data analysis was performed using Python version 3.7.4 and the NumPy version 1.17.4, SciPy version 1.3.1, Pandas version 1.0.3, FlowCal version 1.2.2, and Matplotlib version 3.1.1 libraries. ODE models were simulated using the odeint function of the SciPy.integrate Python package version 1.1 with default parameters. Steady-state response functions of the controllers were calculated by fitting median GFP fluorescence values from the flow cytometry distributions for a range of input IPTG concentrations to the following Hill function

$$y = y_{\min} + (y_{\max} - y_{\min}) \frac{x^n}{K^n + x^n}. \quad (9)$$

Here, y is the output GFP fluorescence in MEFL units, y_{min} and y_{max} are the minimum and maximum output GFP fluorescence in MEFL units, respectively, K is the input IPTG concentration at which the output is half-maximal, n is the Hill coefficient, and x is the input IPTG concentration. Fitting of the experimental data was performed using non-linear least squares and the curve_fit function from the SciPy.integrate package version 1.1. Genetic diagrams were generated using DNAplotlib version 1.0 (Bartoli et al., 2018; Der et al., 2017) and figures were composed using Omnigraffle version 7.15 and Affinity Designer version 1.8.3.

Data availability

Python scripts simulating the ODE models of the direct and multi-level controllers be found in **Supplementary Data 1**. Annotated sequences for all plasmids in GenBank format are available in **Supplementary Data 2**. All plasmids are available from Addgene.

Acknowledgements

This work was supported by BrisSynBio, a BBSRC/EPSRC Synthetic Biology Research Centre grant BB/L01386X/1 (T.E.G., C.S.G.), a Royal Society PhD Studentship (F.V.G.), and a Royal Society University Research Fellowship grant UF160357 (T.E.G.)

Author Contributions

T.E.G. conceived the study. V.G. performed all experiments. T.E.G. developed and simulated the mathematical models. V.G. and T.E.G. analysed the data. T.E.G. and C.S.G. supervised the work. All authors helped to write the manuscript.

Competing Interests

The authors declare no competing interests.

References

Bartoli, V., Dixon, D.O.R., and Gorochowski, T.E. (2018). Automated Visualization of Genetic Designs Using DNAplotlib. In Synthetic Biology: Methods and Protocols, J.C. Braman, ed. (New York, NY: Springer New York), pp. 399–409.

Bartoli, V., Meaker, G.A., di Bernardo, M., and Gorochowski, T.E. (2020). Tunable genetic devices through simultaneous control of transcription and translation. Nat. Commun. *11*, 2095.

Baumschlager, A., Aoki, S.K., and Khammash, M. (2017). Dynamic Blue Light-Inducible T7 RNA Polymerases (Opto-T7RNAPs) for Precise Spatiotemporal Gene Expression Control. ACS Synth. Biol. *6*, 2157–2167.

Beal, J. (2015). Signal-to-Noise Ratio Measures Efficacy of Biological Computing Devices and Circuits. Front. Bioeng. Biotechnol. *3*, 93.

de Boer, H.A., Comstock, L.J., and Vasser, M. (1983). The tac promoter: a functional hybrid derived from the trp and lac promoters. Proc. Natl. Acad. Sci. *80*, 21.

Boo, A., Ellis, T., and Stan, G.-B. (2019). Host-aware synthetic biology. Synth. Biol. *14*, 66–72.

Cameron, D.E., and Collins, J.J. (2014). Tunable protein degradation in bacteria. Nat. Biotechnol. *32*, 1276–1281.

Castillo-Hair, S.M., Sexton, J.T., Landry, B.P., Olson, E.J., Igoshin, O.A., and Tabor, J.J. (2016). FlowCal: A User-Friendly, Open Source Software Tool for Automatically Converting Flow Cytometry Data from Arbitrary to Calibrated Units. ACS Synth. Biol. *5*, 774–780.

Castillo-Hair, S.M., Baerman, E.A., Fujita, M., Igoshin, O.A., and Tabor, J.J. (2019). Optogenetic control of Bacillus subtilis gene expression. Nat. Commun. *10*, 3099.

Ceroni, F., Algar, R., Stan, G.-B., and Ellis, T. (2015). Quantifying cellular capacity identifies gene expression designs with reduced burden. Nat. Methods *12*, 415–418.

Ceroni, F., Boo, A., Furini, S., Gorochowski, T.E., Borkowski, O., Ladak, Y.N., Awan, A.R., Gilbert, C., Stan, G.-B., and Ellis, T. (2018). Burden-driven feedback control of gene expression. Nat. Methods *15*, 387–393.

Chappell, J., Takahashi, M.K., and Lucks, J.B. (2015). Creating small transcription activating RNAs. Nat. Chem. Biol. *11*, 214–220.

518 Chappell, J., Westbrook, A., Verosloff, M., and Lucks, J.B. (2017). Computational design of
519 small transcription activating RNAs for versatile and dynamic gene regulation. Nat. Commun.
520 *8*, 1051.

521 Deng, D., Yan, C., Wu, J., Pan, X., and Yan, N. (2014). Revisiting the TALE repeat. Protein
522 Cell *5*, 297–306.

523 Der, B.S., Glassey, E., Bartley, B.A., Enghuus, C., Goodman, D.B., Gordon, D.B., Voigt, C.A.,
524 and Gorochowski, T.E. (2017). DNAplotlib: Programmable Visualization of Genetic Designs
525 and Associated Data. ACS Synth. Biol. *6*, 1115–1119.

526 Elowitz, M.B., Levine, A.J., Siggia, E.D., and Swain, P.S. (2002). Stochastic Gene Expression
527 in a Single Cell. Science *297*, 1183.

528 Engler, C., Gruetzner, R., Kandzia, R., and Marillonnet, S. (2009). Golden Gate Shuffling: A
529 One-Pot DNA Shuffling Method Based on Type IIs Restriction Enzymes. PLOS ONE *4*, e5553.

530 Gallivan, J.P. (2007). Toward reprogramming bacteria with small molecules and RNA. Curr.
531 Opin. Chem. Biol. *11*, 612–619.

532 Gilbert, L.A., Horlbeck, M.A., Adamson, B., Villalta, J.E., Chen, Y., Whitehead, E.H.,
533 Guimaraes, C., Panning, B., Ploegh, H.L., Bassik, M.C., et al. (2014). Genome-Scale
534 CRISPR-Mediated Control of Gene Repression and Activation. Cell *159*, 647–661.

535 Golding, I., Paulsson, J., Zawilski, S.M., and Cox, E.C. (2005). Real-Time Kinetics of Gene
536 Activity in Individual Bacteria. Cell *123*, 1025–1036.

537 Gomes, L., Monteiro, G., and Mergulhão, F. (2020). The Impact of IPTG Induction on Plasmid
538 Stability and Heterologous Protein Expression by Escherichia coli Biofilms. Int. J. Mol. Sci. *21*.

539 Gorochowski, T.E., van den Berg, E., Kerkman, R., Roubos, J.A., and Bovenberg, R.A.L.
540 (2014). Using Synthetic Biological Parts and Microbioreactors to Explore the Protein
541 Expression Characteristics of Escherichia coli. ACS Synth. Biol. *3*, 129–139.

542 Gorochowski, T.E., Avcilar-Kucukgoze, I., Bovenberg, R.A.L., Roubos, J.A., and Ignatova, Z.
543 (2016). A Minimal Model of Ribosome Allocation Dynamics Captures Trade-offs in Expression
544 between Endogenous and Synthetic Genes. ACS Synth. Biol. *5*, 710–720.

545 Gorochowski, T.E., Grierson, C.S., and di Bernardo, M. (2018). Organization of feed-forward
546 loop motifs reveals architectural principles in natural and engineered networks. Sci. Adv. *4*,
547 eaap9751.

548 Gottesman, S. (2005). Micros for microbes: non-coding regulatory RNAs in bacteria. Trends
549 Genet. *21*, 399–404.

550 Green, A.A., Silver, P.A., Collins, J.J., and Yin, P. (2014). Toehold Switches: De-Novo-
551 Designed Regulators of Gene Expression. Cell *159*, 925–939.

552 Green, A.A., Kim, J., Ma, D., Silver, P.A., Collins, J.J., and Yin, P. (2017). Complex cellular
553 logic computation using ribocomputing devices. Nature *548*, 117.

554 Gyorgy, A., Jiménez, J.I., Yazbek, J., Huang, H.-H., Chung, H., Weiss, R., and Del Vecchio,
555 D. (2015). Isocost Lines Describe the Cellular Economy of Genetic Circuits. Biophys. J. *109*,
556 639–646.

557 Kelly, C.L., Harris, A.W.K., Steel, H., Hancock, E.J., Heap, J.T., and Papachristodoulou, A.
558 (2018). Synthetic negative feedback circuits using engineered small RNAs. Nucleic Acids Res.
559 *46*, 9875–9889.

560 Khalil, A.S., Lu, T.K., Bashor, C.J., Ramirez, C.L., Pyenson, N.C., Joung, J.K., and Collins,
561 J.J. (2012). A Synthetic Biology Framework for Programming Eukaryotic Transcription
562 Functions. Cell *150*, 647–658.

563 Malakar, P., and Venkatesh, K.V. (2012). Effect of substrate and IPTG concentrations on the
564 burden to growth of Escherichia coli on glycerol due to the expression of Lac proteins. Appl.
565 Microbiol. Biotechnol. *93*, 2543–2549.

566 Mangan, S., and Alon, U. (2003). Structure and function of the feed-forward loop network
567 motif. Proc. Natl. Acad. Sci. *100*, 11980.

568 Meyer, A.J., Segall-Shapiro, T.H., Glassey, E., Zhang, J., and Voigt, C.A. (2019). Escherichia
569 coli “Marionette” strains with 12 highly optimized small-molecule sensors. Nat. Chem. Biol. *15*,
570 196–204.

571 Milo, R., Shen-Orr, S., Itzkovitz, S., Kashtan, N., Chklovskii, D., and Alon, U. (2002). Network
572 Motifs: Simple Building Blocks of Complex Networks. Science *298*, 824.

573 Nielsen, A.A.K., Der, B.S., Shin, J., Vaidyanathan, P., Paralanov, V., Strychalski, E.A., Ross,
574 D., Densmore, D., and Voigt, C.A. (2016). Genetic circuit design automation. Science *352*,
575 aac7341.

576 Olson, E.J., Hartsough, L.A., Landry, B.P., Shroff, R., and Tabor, J.J. (2014). Characterizing
577 bacterial gene circuit dynamics with optically programmed gene expression signals. Nat.
578 Methods *11*, 449–455.

579 Raj, A., and van Oudenaarden, A. (2008). Nature, Nurture, or Chance: Stochastic Gene
580 Expression and Its Consequences. Cell *135*, 216–226.

581 Rosano, G.L., and Ceccarelli, E.A. (2014). Recombinant protein expression in Escherichia
582 coli: advances and challenges. Front. Microbiol. *5*, 172.

583 S. Dunn, H. Kugler, and B. Yordanov (2019). Formal Analysis of Network Motifs Links
584 Structure to Function in Biological Programs. IEEE/ACM Trans. Comput. Biol. Bioinform. 1–1.

585 Sen, S., Apurva, D., Satija, R., Siegal, D., and Murray, R.M. (2017). Design of a Toolbox of
586 RNA Thermometers. ACS Synth. Biol. *6*, 1461–1470.

587 Sivashanmugam, A., Murray, V., Cui, C., Zhang, Y., Wang, J., and Li, Q. (2009). Practical
588 protocols for production of very high yields of recombinant proteins using Escherichia coli.
589 Protein Sci. *18*, 936–948.

590 Soper, T., Mandin, P., Majdalani, N., Gottesman, S., and Woodson, S.A. (2010). Positive
591 regulation by small RNAs and the role of Hfq. Proc. Natl. Acad. Sci. *107*, 9602.

592 Storz, G., Opdyke, J.A., and Zhang, A. (2004). Controlling mRNA stability and translation with
593 small, noncoding RNAs. Curr. Opin. Microbiol. *7*, 140–144.

594 Süel, G.M., Garcia-Ojalvo, J., Liberman, L.M., and Elowitz, M.B. (2006). An excitable gene
595 regulatory circuit induces transient cellular differentiation. Nature *440*, 545–550.

596 Waters, L.S., and Storz, G. (2009). Regulatory RNAs in Bacteria. Cell *136*, 615–628.

597 Weiße, A.Y., Oyarzún, D.A., Danos, V., and Swain, P.S. (2015). Mechanistic links between
598 cellular trade-offs, gene expression, and growth. Proc. Natl. Acad. Sci. *112*, E1038.

599 Westbrook, A.M., and Lucks, J.B. (2017). Achieving large dynamic range control of gene
600 expression with a compact RNA transcription–translation regulator. Nucleic Acids Res. *45*,
601 5614–5624.

602 Woodruff, L.B.A., Gorochowski, T.E., Roehner, N., Mikkelsen, T.S., Densmore, D., Gordon,
603 D.B., Nicol, R., and Voigt, C.A. (2016). Registry in a tube: multiplexed pools of retrievable
604 parts for genetic design space exploration. Nucleic Acids Res. *45*, 1553–1565.

Tables

Table 1: Performance summary of the single- and multi-level controllers[a]

Controller	Type[b]	Dynamic range[c] (10^3 MEFL)	Fold change[c]	Cooperativity[d], *n*	Signal to Noise Ratio (dB)
P_{tac}	SLC	0.9	93	3.4	0.2
THS	MLC	65.5	2166	7.3	10.1
STAR	MLC	4.6	53	9.3	4.7
$STAR_2$	MLC	3.4	37	7.7	4.5
DC	MLC	10.4	1030	3.4	7.1

a. All values are averages calculated from three biological replicates.
b. SLC refers to 'single-level controller' and MLC refers to 'multi-level controller'.
c. Calculated between 'on' and 'off' states for cells grown in 0 and 1 mM IPTG, respectively, and given in calibrated molecules of equivalent fluorescein (MEFL) units.
d. From the Hill function fitting of the steady state response functions (**Figure 4A**; **Supplementary Figure 2**).

Figures and captions

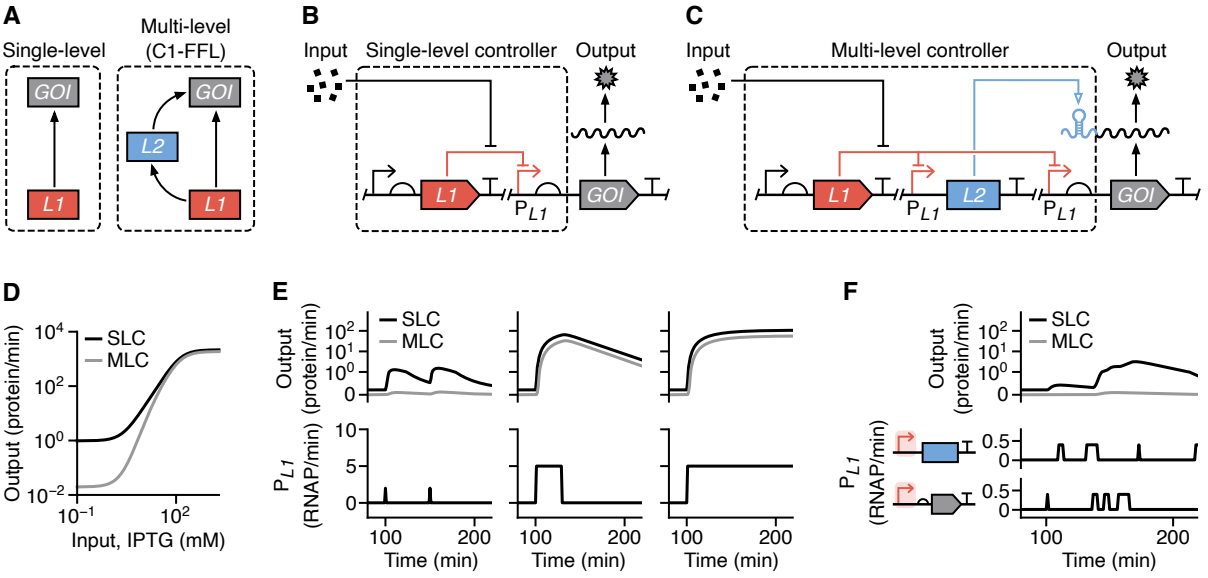

Figure 1: Stringent control of protein expression through multi-level gene regulation. (**A**) Two possible regulatory schemes to control the expression of a gene of interest (GOI): 1. control using a single regulator (*L1*), and 2. multi-level control using two separate regulators (*L1* and *L2*) connected in the form of a coherent type 1 feed-forward loop (C1-FFL). (**B**) Schematic of a genetic implementation of a single-level controller (SLC) that uses only transcriptional (red lines) regulation. An input (e.g. small molecule) modulates activity of the P_{L1} promoter and production of the GOI. (**C**) Schematic of a genetic implementation of a multi-level controller (MLC) that uses both transcriptional (red lines) and translational (blue line) regulation. An input (e.g. small molecule) modulates activity of the two P_{L1} promoters and an internal *L2* regulator activates the translation of GOI transcripts to finally produce the output protein. (**D**) Steady state response functions from mathematical models of the SLC and MLC. (**E**) Dynamic model simulations of the SLC and MLC and their response to different forms of temporal input (left to right): short pulses (P_{L1} activity = 2 RNAP/min for 1 min at 100 min and 150 min), square wave (P_{L1} activity = 5 RNAP/min from 100–130 min), and a step function (P_{L1} activity = 5 RNAP/min from 100 min onwards). The activity of both P_{L1} promoters in the MLC is considered identical. (**F**) Dynamic model simulations of the SLC and MLC showing suppression of intrinsic promoter noise by the MLC. The two identical P_{L1} promoters for the *L2* regulator and GOI are separately driven by independent and biologically realistic bursty transcriptional activity profiles (**Methods**).

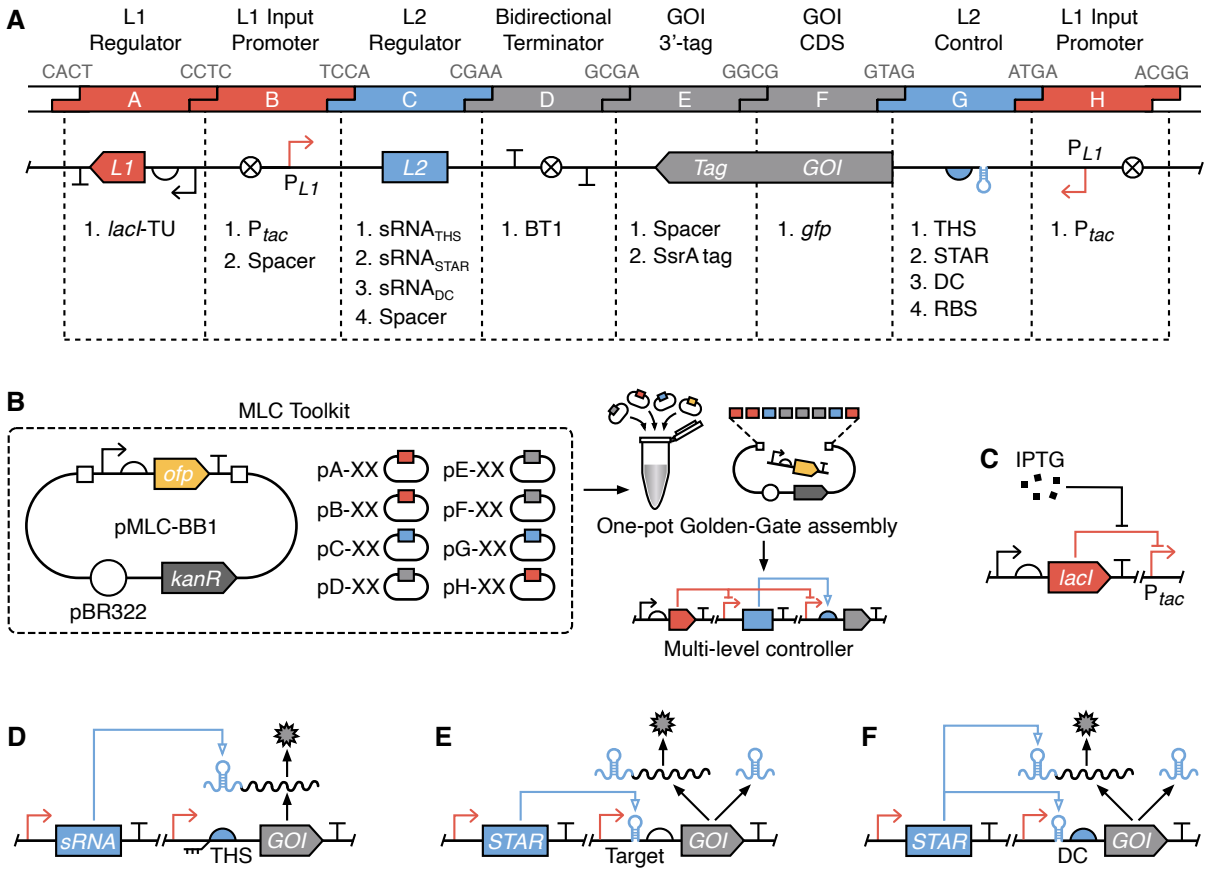

Figure 2: Combinatorial assembly of gene expression controllers. (**A**) Summary of the 8-part genetic template used to allow for systematic exploration of direct and multi-level gene regulation. The 4 bp overhangs used for Golden-Gate assembly are shown in grey at their respective junctions. Available genetic elements are listed below each corresponding part type (A–H). (**B**) The MLC toolkit contains a set of plasmids that can be combined using Golden-Gate assembly to create a variety of direct and multi-level controllers (**Supplementary Figure 3**). (**C**) The *lacI* transcription factor responsive to IPTG used for level 1 (*L1*) transcriptional regulatory control. (**D**) Toehold switch (THS) translational regulator used for level 2 (*L2*) control. (**E**) Small transcription activating RNA (STAR) transcriptional regulator used for *L2* control. (**F**) Dual control (DC) transcriptional and translational regulator used for *L2* control.

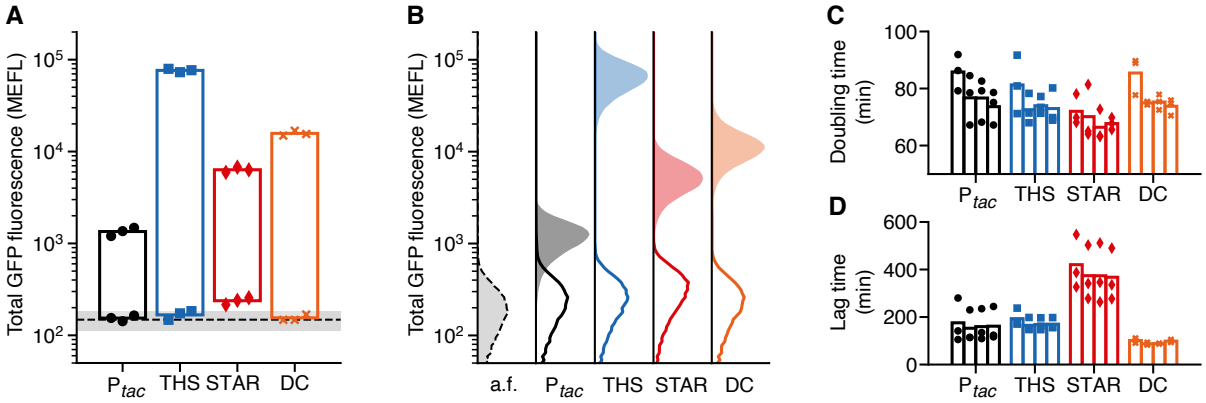

Figure 3: Performance comparison of single- and multi-level controllers. (**A**) Total GFP fluorescence for 'off' and 'on' input states (0 and 1 mM IPTG, respectively). Points show the three biological replicates for each controller and condition (black circles, P_{tac}; blue squares, THS; red diamonds, STAR; orange crosses, DC). Black dashed line denotes the mean fluorescence of cell autofluorescence (a.f.) controls containing no plasmid with grey shaded region showing ± 1 standard deviation of 11 biological replicates. Fluorescence given in calibrated molecules of equivalent fluorescein (MEFL) units. (**B**) Flow cytometry distributions of total GFP fluorescence for 'off' (line) and 'on' (shaded) input states. Cell autofluorescence (a.f.) controls containing no controller are shown by black dashed line and light grey filled distributions. (**C**) Doubling time of cells harbouring direct and multi-level controllers for varying concentrations of IPTG (bars left to right for each design: 0, 0.1, 1, 10 mM IPTG). (**D**) Lag time calculated as the time to reach an OD_{600} = 0.15 after inoculation of cells harbouring controllers for varying concentrations of IPTG (bars left to right for each design: 0, 0.1, 1, 10 mM IPTG).

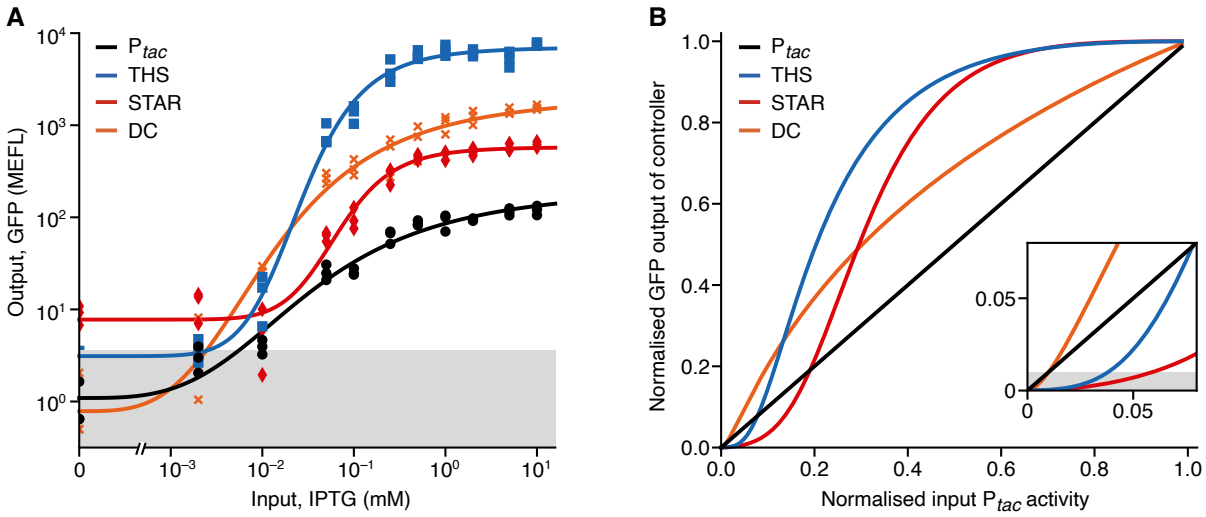

Figure 4: Response functions of single- and multi-level controllers. (**A**) Steady state response functions of the controllers showing output GFP fluorescence (corrected for cell autofluorescence) for varying input IPTG concentrations (0, 0.002, 0.01, 0.05, 0.1, 0.25, 0.5, 1, 2, 5, 10 mM). Points show the three biological replicates for each controller and condition (black circles, P_{tac}; blue squares, THS; red diamonds, STAR; orange crosses, DC). Grey shaded region shows the standard deviation of cellular GFP autofluorescence from 11 biological replicates. (**B**) Comparison of how normalised GFP output (as a fraction of the maximum GFP fluorescence) varies in response to changes in the normalised transcriptional activity of P_{tac} (as a fraction of its maximum activity). Multi-level regulation can lead to the suppression or amplification of the output GFP production rate compared to direct transcriptional regulation (i.e. a specific multi-level controller's line falls below or above the diagonal, respectively). Insert shows zoomed area and grey shaded region denotes a GFP output level of 1% for the controller.